Integrated sensors to experimentally measure microheater uniformity: geometry implications in meander-based structures.

Calderon-Gonzalez M., Cheyns D., Ameloot R., and Genoe J., *Member, IEEE.*

***Abstract*— Microheaters have evolved to become a key component of devices in a wide range of applications, many of which require a thermal profile with good uniformity. To this end, it is critical not only to select an appropriate device geometry but also to have reliable tools to assess the uniformity in the microscale. This paper presents a collection of novel sensors to experimentally extract the mean temperature in various regions of the micro-hotplate with high accuracy, offering an innovative alternative to other uniformity measurement tools that are often not available or not sufficiently precise. The studies are articulated around a series of meander-based microheaters, for which the temperature versus voltage profile, response time, power consumption and uniformity are studied. In this way, insight into the influence of different geometrical parameters (i.e. line arrangement, scaling, linewidth and line spacing) is provided. Finite Element Method simulations are performed based on certain assumptions and boundary conditions and exhibit strong concordance with our experimental data, thus we demonstrated that the sensors serve as a tool to validate the representativeness of a model.**

***Index Terms*— Microheater uniformity, microheater design, meander, temperature sensors, Finite Element Method simulations.**

I. INTRODUCTION

MINIATURIZED heating devices are becoming increasingly popular as they can play a pivotal role in a wide number of applications [1], [2], [3], with special interest being placed in the development of bendable microheaters [2], [4], [5], [6]. Compared with their bulk counterparts, microheaters benefit from greater portability, lower power consumption, a wider temperature range, faster response time, and reduced costs. The properties of micro-hotplates are highly dependent on factors such as selected materials, design, substrate, heater configuration (closed, partially closed, or suspended membrane), and processing techniques [7], [8]. Among these factors, the micro hotplate design has a major impact on the thermal profile, response time and power consumption.

We thank the Research Foundation Flanders (FWO Vlaanderen) for funding in the research project G087422N.

Maider Calderon Gonzalez and Jan Genoe are with the Department of Sensors and Actuators (SAT) at imec, 3001 Leuven, Belgium; and with the Electrical Engineering (ESAT) department at KU Leuven, 3590 Diepenbeek, Belgium, (e-mail: maider.calderongonzalez@imec.be, jan.genoe@imec.be)

David Cheyns is also with SAT at imec, 3001 Leuven, Belgium (e-mail: david.cheyns@imec.be)

Rob Ameloot is with the Department of Microbial and Molecular Systems at KU Leuven, 3001 Leuven (e-mail: rob.ameloot@kuleuven.be)

For applications in which high uniformity is required, is essential not only to select a suitable microheater geometry but also to have appropriate methods to reliably extract the thermal profile. As a tool for predicting and optimizing heater characteristics, accurate analytical models have been developed [9]. Yet, the undeniable superiority of Finite Element Method (FEM) simulations in terms of accuracy has made this methodology to be particularly popular in this field [4], [5], [6], [10], [11], [12], [13], [14], [15], [16], [17], [18], [19]. To obtain reliable simulations, it is necessary to achieve precise knowledge of the system with respect to the heat propagation mechanisms (convection, conduction, and radiation). Ideally, these parameters should not be taken from literature or previous work since experimental conditions may vary, however, their experimental extraction is not simple. As a result, common practices consist of assumptions [8], [20], which may lead to inaccurate simulations. Thus, to fully confirm the veracity of a simulation for a given system, its subsequent experimental evaluation is of utmost importance, as observed in the literature [5].

To experimentally extract the temperature profile at the micro-scale with high accuracy and resolution, non-contact techniques such as Raman thermometry and electron energy loss spectroscopy are used, but their availability in the lab is often limited [21]. Alternatively, infrared cameras are commonly used as non-contact method, but they can show strong dependencies on material emissivity and insufficiencies in precision [21], [22]. In contrast, contact methods for temperature measurement consist of thermistors, thermodiodes and thermocouples. Interestingly, microheaters and thermistors are closely related: similar structures can be used as heat sources or as resistance-based temperature sensors [22], [23], [24], [25]. This attractive phenomenon can be exploited to measure the temperature of a microheater. In the work of Lu *et al.*, a meander-shaped Pt sensor is introduced on top of a microheater to measure its average temperature [11]. In addition, it has been shown that the operation mode of a given structure can be switched between a microheater and a temperature sensor [26]. Although these contact methods provide useful information, they are mainly used to ascertain average temperatures and not yet as a methodology to obtain information on how the temperature is distributed spatially, i.e. the microheater uniformity.

Regarding microheater design selection, novel structures with a certain degree of complexity have been studied [10], [11], however, it is common for researchers to select simpler structures that are easier to fabricate, consisting of meanders

and spirals [12], [13], [27]. The performance and characteristics of microheaters with different structures have been widely compared in the literature [14], [15], [16], [17], [18], [28]. Nonetheless, the conclusions drawn by these comparisons must be considered with caution as these devices often possess different dimensions, a distinct width or spacing of the heating lines, or other variations that make the contrast not straightforward. Little work has been done to understand how different geometric parameters influence the characteristics of a heater with a given structure. Gayake *et al.* studied the variation of the width and the spacing in the heater, but at the expense of modifying the size accordingly [16]. In this regard, Paun *et al.* compared two equivalent meanders with distinct widths only by simulations [19]. Therefore, there is still a need to develop more comprehensive and systematic studies in which the different geometric parameters (size, arrangement, spacing, and width) are studied in a more independent manner.

The aim of this paper is to demonstrate novel temperature sensors that will give insight into the experimental uniformity of micro hotplates. Contrary to the current trends in the literature where the average temperature of the whole active area is measured, we propose using a set of resistive-based sensors that will allow us to accurately measure the average temperature of more discrete regions. As one of the main sources of thermal inhomogeneity is the thermal loss in the heater periphery, we propose to design the sensors as such to measure the average temperature of regions which a selected distance from the microheater sides. Sensors are placed on the heater surface (on-top sensors) which will provide experimental insight into the microheater uniformity. Furthermore, the experimental data obtained by these sensors is used to validate the representativeness of the performed FEM simulations. For this purpose, we additionally propose the use of spaced sensors in regions around the heater (in-plane sensors), which will allow us to verify the surrounding temperature [29], [30]. Therefore, in-plane sensors will serve as a complementary tool to scrutinize the assumptions made in the FEM model, more specifically, those related to heat conduction along the insulator. Our studies are built around a series of meander-like micro hotplates, an architecture that leads to devices with high performance yet making use of a simple design. Aiming to provide a more thorough insight into the influence of the geometrical parameters, a series of heaters were judiciously designed and fabricated with A) equivalent resistance and variable line arrangement, B) equivalent resistance and variable scaling, C) equivalent area and variable line spacing, and D) equivalent area and variable line width. Notably, by employing series C) and D) we study the influence of linewidth or line spacing decoupled from size effects, an approach that has not been found yet in the literature. Platinum is chosen as a heating/sensing material due to its widely known ideal characteristics [7], whereas polyimide (PI) will act as an insulator so as to enable flexible applications and as a result of its low thermal conductivity, and stability [5], [7].

II. FABRICATION AND METHODS

A. Fabrication

A schematic of the final device stack is shown in Fig. 1a, which was fabricated as follows. On a 6-inch glass wafer, a ~15 μm film of PI (PI2611, HD Microsystems) was obtained by spin coating at 750 rpm and curing the film at a temperature up to 350 ºC. Subsequently, a 100 nm thick sputtered platinum film was patterned by a lift-off technique to form the microheater structures and on-plane sensors. Next, photo-patternable PI (HD4100, HD Microsystems) was spin coated at 3000 rpm, exposed, and cured at 270 ºC. This allowed us to obtain a 5 μm film with open vias for direct contact with the heater structures, without using contact electrodes. Finally, the sensors on top of the heater structure were fabricated through the deposition and lift-off of 100 nm thick sputtered platinum. We found good adhesion of the platinum layers to both types of PI films, so no adhesion promoters were required.

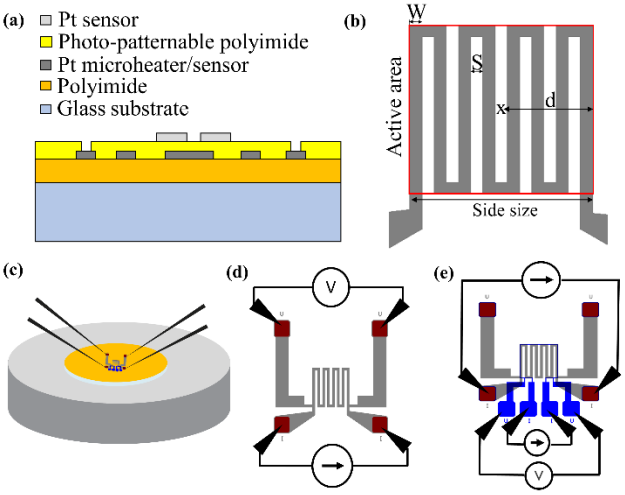

Fig. 1. **(a)** Cross-sectional view of the microheaters. **(b)** Top view of a reference microheater with W the width of the heating line, S the spacing between lines, x the central point of the device, and d the distance between x and heater edge in the x-direction. The device's active area is marked as a red square. **(c)** Experimental set-up. Measurements are performed in a temperature-modulated chuck maintained at 25 ºC. **(d)** Measurement layout for the extraction of microheater characteristics using 4-probe method. **(e)** Layout for sensor-related experiments using the 4-probe method. This set-up applies to both on-top and in-plane sensors.

B. Experimental measurements

B.1 Microheater measurements

The resistance of Pt increases linearly with the temperature [7], following the equation

$$R = R_{ref}\left[1+\alpha\left(T-T_{ref}\right)\right] \qquad (1)$$

where R_{ref} is the reference resistance at a reference temperature T_{ref}, R is the resistance at a given temperature T, and α is the Temperature Coefficient of Resistance (TCR). Hence, by measuring the resistance, R, of the heaters, their

average temperature can be easily calculated if the rest of the parameters are known. To experimentally extract α, the resistance was measured by applying a small current of 1 mA, which ensures that no self-heating (Joule heating) occurs. Using a probe station with a temperature-modulated chuck (FormFactor's Cascade PA300), we recorded the different resistances at temperatures ranging from 15 to 150 ºC. To obtain reliable measurements is critical to use the 4-point probe method to eliminate the influence of contact resistance (see Fig. 1d). We measured different devices, finding α = 0.0025 ± 0.0001 $ºC^{-1}$. With this information we can relate the measured resistance of the heater to its temperature at different applied voltages (temperature vs voltage profile). Because of limitations coming from the PI, the upper-temperature limit is set at 250 ºC. The response time of the devices was obtained by measuring the resistance as a function of time at 10 ms intervals. Typically, the resistance increases rapidly in the first milliseconds of the measurement until reaching a stable and constant saturation point, or steady state. The power per active area, sometimes named power density [5], is calculated at the saturation point by dividing the product of voltage and current by the active area of the heater. We consider the response time as the time required to reach 97% of the saturation temperature. It is important to note that all microheater characterization measurements were performed in a closed probe station equipped with a temperature-modulated chuck This chuck is maintained at 25 ºC, which we take as temperature of reference (see Fig. 1c). To obtain the measurement errors, a minimum of three different devices are evaluated.

B.2 Sensor measurements

Comparable to microheaters, the sensor readouts are based on resistance measurements and follow (1). Using the previously described method, TCR was calculated to be α = 0.0025 ± 0.0001 $ºC^{-1}$ for in-plane sensors, and α = 0.0021 ± 0.0001 $ºC^{-1}$ for the on-top sensors. This difference in the value corresponds to the fact that the devices are in distinct surroundings, and variables such as the PI roughness play a role. Due to limitations of number of available probes, the 4-probe method was now limited to merely the sensors, assuming that the microheater characteristics are well known from the previous section. For the scope of this proof-of-concept, thermal sensors are set to measure the temperature in the steady state, however, transient studies could also be considered. Fig. 1e shows the measurement layout, which can be used for both types of thermal sensors (i.e. on-top and in-plane). Firstly, the reference resistance of each sensor is obtained by applying a low current of 0.5mA, ensuring no Joule heating in the sensor. Then, the microheater is turned on by supplying the desired current and subsequently, the resistance of the thermal sensor is again recorded. Typically, the resistance (and hence the temperature) of the both on-top and in-plane sensor are maintained throughout the time, thus confirming that we have reached a steady state.

Several replicas for a given microheater are fabricated within the same wafer, each of them provided with a certain heat sensor. A minimum of three replicas of a given sensor are evaluated to calculate measurement deviation. Heat sensors have a width of 10 µm, and they are placed either in the plane with the heater or on top of the heater covering a region which is equidistant from the active area edges, as represented in Fig. 2. On-top sensors (Fig. 2a and Fig. 2c) are always placed at 100, 150, and 225 µm in the x and y direction from the hotplate center for the groups of heaters with similar areas (Series C, and D). However, to be able to compare the samples in Series A, and B due to their variable dimension, the position of on-top sensors is set to be at the distances *d* and *d/2* from the heater center. In-plane sensors (Fig. 2b and Fig. 2d) are always placed at 50, 100, 150, 200, and 250 µm from the active area edges independently of the design. For our study, we assume that the influence of the sensors on the microheater is negligible.

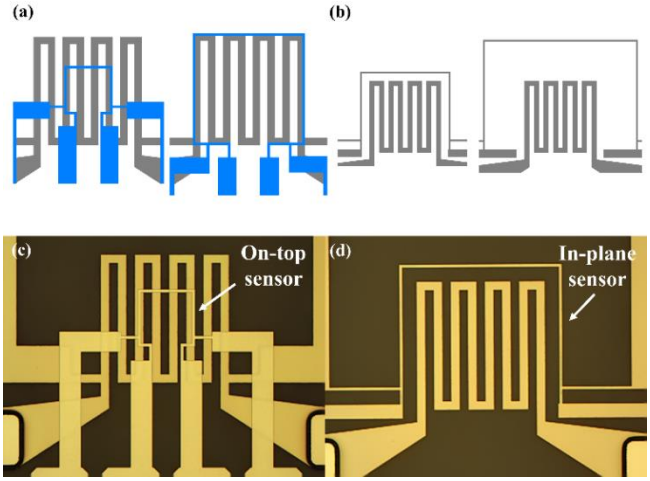

Fig. 2. Layout and microscope images of the reference microheater and associated sensors. **(a)** Layout of the smallest (100 µm) and largest (225 µm) on-top sensor, represented in blue on top of the microheater. **(b)** Layout of the smallest (50 µm) and largest (250 µm) in-plane sensor, represented with the same color as the microheater. **(c)** Microscope image of the smallest on-top sensor. **(d)** Microscope image of the smallest in-plane sensor.

C. Simulation model

FEM simulations were performed using COMSOL Multiphysics software, with the electromagnetic heating (Joule Heating) Multiphysics module. The total area under study was limited to an area of 0.5 cm^2, in the center of which the microheater is located. The thickness of the modelled materials corresponds to the experimental values (see Section II.A). Most of the material's physical parameters were taken from the COMSOL material library (Table I). In the case of the platinum, we provided the values of reference resistivity (ρ_0 =1.9E-7 Ωm) at a reference temperature (298 K), and the resistivity temperature coefficient (α = 0.0025 $ºC^{-1}$), which were obtained experimentally.

The electromagnetic heating Multiphysics module couples the electric currents and heat transfer in solids modules, governed by the following equations:

TABLE I
MATERIALS PROPERTIES AT COMSOL LIBRARY

Material properties	Polyimide	Platinum	Glass
Heat capacity, J/ (Kg K)	1100	133	730
Density, Kg/m^3	1300	21450	2210
Thermal conductivity, W/ (m K)	0.15	71.6	1.4
Electrical conductivity, S/m	6.67	*	1e-14
Relative permittivity	3.4	1	4.2

* The model derives the electrical conductivity of platinum from the provided experimental resistivity and thermal coefficient of resistance.

$$\rho\, C_p \frac{\partial T}{\partial t} - \nabla(k \nabla T) = Q_e \tag{2}$$

$$Q_e = J\, E \tag{3}$$

where ρ accounts for density, C_p for specific heat, T is absolute temperature, k is the thermal conductivity of the medium, Q_e represents the resistive losses, J is the current density and E is the electric field. For the case of the electrical currents, we use a linearized resistivity model, in which the conductivity σ varies in function of the temperature.

$$J = \sigma\, E \tag{4}$$

$$\sigma = \frac{1}{\rho_0 \left[1+\alpha\,(T-T_{ref}) \right]} \tag{5}$$

In the case of heating and for the top surface, we are considering a convective heat flux (6) and surface-to ambient radiation (7).

$$-n\, q = h\,(T_{amb}-T) \tag{6}$$

$$-n\, q = \varepsilon\, \sigma_{sb}\,(T_{amb}^4-T^4) \tag{7}$$

Where n is the normal vector, q is conductive heat flux vector, h is the heat transfer coefficient, T_{amb}, the ambient temperature, ε is emissivity and σ_{sb} is the Stefan-Boltzmann constant. Due to the low emissivity of platinum, we only consider the polyimide emissivity with ε = 0.75, and we assume natural free convection with h = 10 W/(m^2 K). As boundary conditions the ambient temperature, initial temperature, and temperature of the rest of the surfaces in the model are considered to have a value of 298 K. For these simulations a tetrahedral mesh is built.

III. RESULTS AND DISCUSSION

A. Microheater thermal characteristics

Four different series of heaters were designed and fabricated, divided into two main groups. The first group includes sets of devices with equivalent resistance (Series A, and B). The resistance can be defined as the following:

$$R = R_s \frac{W}{L} \tag{8}$$

where R_s is the sheet resistance, used commonly to compare the resistance of thin films with the same thickness; and W/L is the ratio of width versus length, which is widely known as *number of squares.* The total length L, of the device is calculated by summing the lengths of its constituent metallic lines in the active area. Since the heaters and sensors in this paper are made of the same material and thickness, they have comparable R_s. Consequently, micro-hotplates with equivalent resistance can be obtained by meticulously selecting geometric parameters that lead to the same W/L ratio, regardless of device size or arrangement. This group of devices allows to study the influence of number of lines (Series A) and scaling (Series B) on the thermal characteristics of the devices. The second group consists of microheaters with comparable active areas (Series C, and D). The purpose of this group is to study the influence of the spacing (Series C) and the width of the heating lines (Series D). The geometric parameters used for the design of each microheater are summarized in Table II. As reference structure, we have chosen a sample with 8 heating lines, 450 µm side size, 30 µm linewidth, and 30 µm line spacing, which is included in each of the microheater sets. Besides, we define d as the distance from the hotplate centre to the edge in the x-direction (see Fig. 1). This parameter, which is also included in Table II, will serve especially of use in the discussion of the simulations results.

A.1 Influence of arrangement: Number of lines

The characteristics of the Series A of heaters (equivalent resistance and variable number of lines) are compared and shown in Fig. 3. The set of devices is composed of structures with 6, 8, 10, 12 and 20 lines, whose designs are shown in Fig. 3a. Note that all geometries possess a different aspect ratio, which is defined by the ratio between heater's side size in the x-direction to the side size in the y-direction. The temperature versus voltage profile of these devices (Fig. 3b) can be fitted to a quadratic curve, coming from the fact that the device temperature (T) increases proportionally with the dissipated electrical power (P), which is the product of voltage (V) and current (I); and considering Ohm's law:

$$T \propto P = I\, V = \frac{V^2}{R} = I^2\, R \tag{9}$$

The temperature of equilibrium is reached when the system is in a steady state in which all heat contributions are balanced: the resistive heat produced by the heater equals the heat dissipated by convection, conduction, and radiation, whereas no more heat is consumed to raise the temperature. The time it takes for this process to be satisfied is faster at lower temperatures as is closer to the initial state (see Fig. 3c). However, at higher temperatures the response time becomes rather independent. This could be attributed to a more significant transient heat consumption, which is the responsible to raise the device temperature, with respect to the transient heat dissipation. The power consumption per active area, calculated in the steady state point, increases linearly with the temperature following (9) and is shown in Fig. 3d.

TABLE II

OVERVIEW OF THE STUDIED HEATERS WITH THEIR CORRESPONDING GEOMETRIC PARAMETERS

Series A: Heaters with equivalent resistance and variable arrangement (Number of lines)

Device distinction	Area (µm x µm)	Number of lines	Number of squares	Line spacing (µm)	Line width (µm)	Distance of heater center to edge, *d* (µm)	Position of on-top sensors (µm)
6 lines	330 x 610	**6**	127	30	30	165	83, 165
8 lines (REF)	450 x 450	**8**	127	30	30	225	113, 225
10 lines	570 x 354	**10**	127	30	30	285	143, 285
12 lines	690 x 290	**12**	127	30	30	345	173, 345
20 lines	1170 x 162	**20**	127	30	30	585	293, 585

Series B: Heaters with equivalent resistance and variable size (Scaling)

Device distinction	Area (µm x µm)	Number of lines	Number of squares	Line spacing (µm)	Line width (µm)	Distance of heater center to edge, *d* (µm)	Position of on-top sensors (µm)
300 µm side size	**300 x 300**	8	127	20	20	150	75, 150
450 µm side size (REF)	**450 x 450**	8	127	30	30	225	123, 225
525 µm side size	**525 x 525**	8	127	35	35	253	126, 252
600 µm side size	**600 x 600**	8	127	40	40	300	150, 300
750 µm side size	**750 x 750**	8	127	50	50	375	188, 375
900 µm side size	**900 x 900**	8	127	60	60	450	225, 450

Series C: Heaters with equivalent area and variable spacing (Spacing)

Device distinction	Area (µm x µm)	Number of lines	Number of squares	Line spacing (µm)	Line width (µm)	Distance of heater center to edge, *d* (µm)	Position of on-top sensors (µm)
2 µm spacing	446 x 450	14	211	**2**	30	223	100, 150, 225
8 µm spacing	448 x 450	12	183	**8**	30	224	100, 150, 225
17 µm spacing	453 x 450	10	155	**17**	30	227	100, 150, 225
30 µm spacing (REF)	450 x 450	8	127	**30**	30	225	100, 150, 225
54 µm spacing	450 x 450	6	99	**54**	30	225	100, 150, 225
110 µm spacing	450 x 450	4	71	**110**	30	225	100, 150, 225

Series D: Heaters with equivalent area and variable width (Width)

Device distinction	Area (µm x µm)	Number of lines	Number of squares	Line spacing (µm)	Line width (µm)	Distance of heater center to edge, *d* (µm)	Position of on-top sensors (µm)
4 µm width	446 x 450	14	1673	30	**4**	223	100, 150, 225
10 µm width	450 x 450	12	573	30	**10**	225	100, 150, 225
18 µm width	450 x 450	10	265	30	**18**	225	100, 150, 225
30 µm width (REF)	450 x 450	8	127	30	**30**	225	100, 150, 225
50 µm width	450 x 450	6	57	30	**50**	225	100, 150, 225

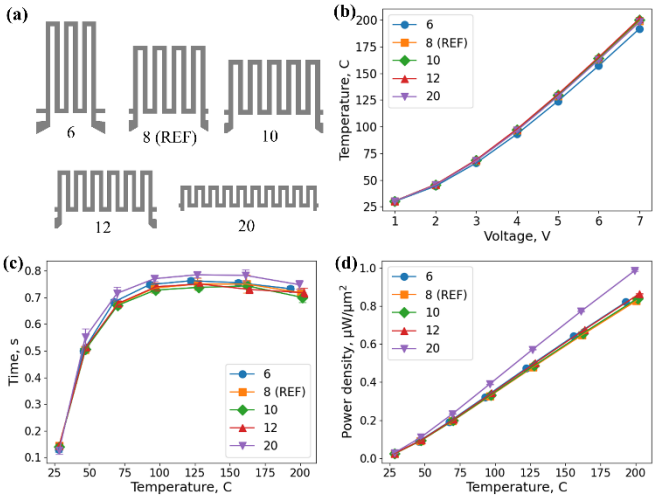

Fig. 3. Influence of microheater arrangement. **(a)** Layout of the different designs, which consists of microheaters based on 6, 8, 10, 12, and 20 lines **(b)** Temperature versus voltage profiles. **(c)** Response time. **(d)** Power consumption per µm^2.

In general, all microheaters exhibit similar characteristics, suggesting that the arrangement of the heating lines does not have a large impact. Exceptionally, the 20-line microheater, which possesses the largest aspect ratio, shows a considerable deviation regarding power consumption. This phenomenon can be explained by considering the perimeter of each device: while for most of the heaters is between 900-980 µm, for the 20-line microheater is larger than 1300 µm. This device establishes a larger contact with cold regions, resulting in more power consumption due to an increased heat conduction through the PI. Consequently, heat is poorly confined in the active area.

A.2 Influence of scaling

To study the influence of the scaling, we use Series B, which is composed of heaters with equivalent resistance and variable size (Fig. 4). The set of samples consists of structures with 300, 450, 525, 600, 750 and 900 µm side size, and the designs are shown in Fig. 4a. Although the resistance of the heater is comparable in all devices, the larger a microheater is, the larger the voltage (Fig. 4b) and the longer time (Fig. 4c) it takes to reach a given temperature. This can be explained through the concept of *thermal mass*, which depends on the heater size and heat insulation and defines the capacity of a micro-hotplate to increase its temperature and store heat efficiently. A heater with an increased thermal mass (i.e. the

larger heater) requires more "effort" in terms of energy and time to increase its temperature. Additionally, heat dissipation mechanisms (conduction, convection, and radiation) are area-dependent, leading to an increased absolute power consumption in more bulky devices. Nonetheless, if power consumption per active area is considered (Fig. 4d), it is seen that the power consumption of smaller devices is greater. This implies that devices with reduced size are less efficient compared with their large counterparts, a fact known in the literature [8]. In practice, for a rapid heating of large areas is preferable to use an array of small microheaters rather than a single large device [31], [32]. However, if for a given application it is necessary to heat a large area with limited power consumption, it is shown that is more convenient to use a large microheater rather than an array of small hotplates, but at the expense of a longer response time.

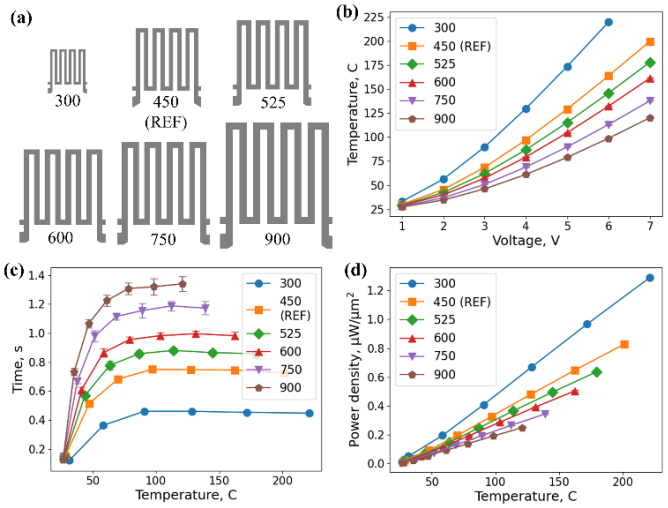

Fig. 4. Influence of microheater scaling. **(a)** Layout of the different designs, which consists of microheaters based on 300, 450, 525, 600, 750, and 900 μm side size. **(b)** Temperature versus voltage profiles. **(c)** Response time. **(d)** Power consumption per μm^2.

A.3 Influence of spacing

Fig. 5 shows results obtained for the set of heaters with equivalent area and variable line spacing (Series C). To maintain an equivalent area in the set excluding size effects, the reduction in spacing is accompanied by an increase in the number of lines, therefore the resistance of the devices increases accordingly. This series of microheaters is composed by structures with 2, 8, 17, 30, 54 and 110 μm spacing (Fig. 5a). For a given voltage and following (9) more resistive devices reach less temperature, which is in good agreement with what is shown in Fig. 5b. The power consumption of the device in equilibrium is the result of the conduction, convection, and radiation of the system, which are known to be area-dependent mechanisms. Accordingly, devices with similar active areas show similar power consumption characteristics regardless of their spacing or resistance, as demonstrated in Fig. 5d. The response time, on the contrary, depends on transient behavior of not only the power dissipation mechanisms but also the ability to increase the temperature. Interestingly, Fig. 5c demonstrates a similar response from all the devices, which indicates that the variations in spacing and resistance, and thus the amount of heating material, do not have a large impact if the dimensions of the active area are maintained.

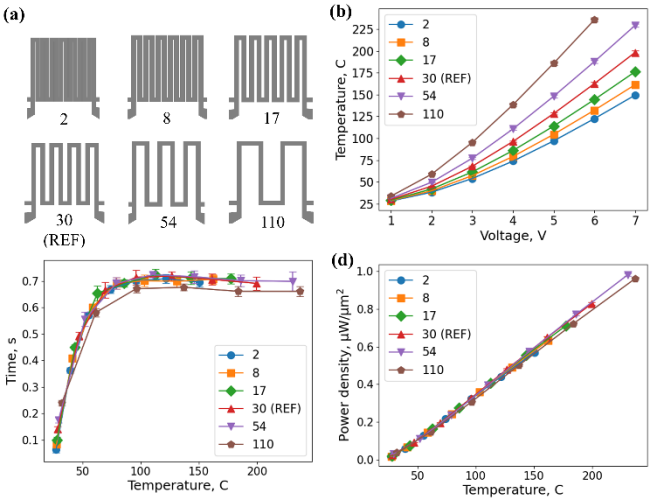

Fig. 5. Influence of microheater line spacing. **(a)** Layout of the different designs, which consists of microheaters based on 2, 8, 17, 30, 54, and 110 μm spacing. **(b)** Temperature versus voltage profiles. **(c)** Response time. **(d)** Power consumption per μm^2.

A.4 Influence of linewidth

The influence of heater linewidth is studied by the Series D, a set of samples with equivalent area (which eliminate size effects) but variable width and is shown in Fig. 6. This series of devices is composed by structures with 4, 10, 18, 30 and 50 μm linewidth (Fig. 6a).

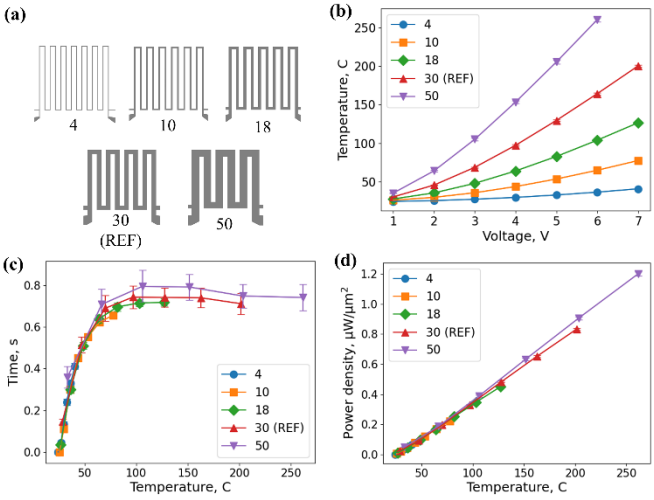

Fig. 6. Influence of microheater linewidth. **(a)** Layout of the different designs, which consists of microheaters based on 4, 10, 18, 30 and 50 μm width. **(b)** Temperature versus voltage profiles. **(c)** Response time. **(d)** Power consumption per μm^2.

As in the previous case, the resistance of the microheaters is varying from heater to heater, so the same trend can be seen in Fig. 6b: less resistive samples achieve higher temperatures at a given voltage. In a similar fashion, the response time (Fig. 6c) and power density (Fig. 6d) are not strongly influenced by

the linewidth and resistance and, consequently, by the amount of heating material. Accordingly, one could argue that wider-line structures are preferable, as they can achieve a broader range of temperatures with less applied voltage, maintaining the time response and power consumption. However, devices with reduced resistance (larger linewidth) will suffer from higher current densities at a given voltage. This fact, as seen in the literature, may lead to problems of electromigration and lifetime [33], therefore a vast increase in linewidth is not recommended.

B. Experimental uniformity using on-top sensors

The uniformity of a heater reflects the degree of temperature homogeneity in the active area. For certain applications, a high degree of uniformity is of utmost importance. Two main aspects play a role in the uniformity of a microheater: the presence of hotspots, and the edge effect. Hotspots arise from temperature differences in regions with a heating line or space underneath. Therefore, hotspots could be reduced by increasing the thickness of the insulator or using insulating materials with low thermal conductivity which will result in a better heat distribution. On the contrary, the edge effect comes from the temperature difference of the hotplate and its surroundings, causing the periphery of the active area to have a reduced temperature as a result of favored heat conduction.

The average temperature at the selected regions in the heater area was experimentally extracted by on-top heat sensors. Note that these sensors are designed with a square shape (see Fig. 2), therefore we expect a higher sensitivity to edge effect contributions. However, the presence of hotspots will also be influencing the system, as the sensor cross through heating lines and spacings multiple times in the x-direction. To compare the uniformity of each device using the known sensor temperatures, we propose to use the *coefficient of variation (CV)*, which defines the extent of dispersion of a value around its average:

$$Uniformity = 1\text{-}CV = 1\text{-}\frac{\sigma_T}{\mu_T} \qquad (10)$$

where μ_T is the average value of the temperatures obtained by the different heat sensors, and σ_T is the standard deviation. Fig. 7 shows the uniformity values as a function of the device temperature, where a general decrease in uniformity is observed with increasing temperature. As mentioned above, an identical reference microheater was included in each set of devices, which can be referred to as one of the following depending on the set: 8-line microheater, 450 µm side microheater, 30 µm spacing microheater and/or 30 µm width microheater. Comparing the uniformity values of this specific sample, we observe a variation in the uniformity value: ~ 0.850 or ~ 0.875 depending on the set studied. The explanation lies in the number of sensors considered for the study (two for heaters with equal resistance, and three for heaters with equal area). The more sensors considered, the more accurate the uniformity value is expected to be. As a consequence, the uniformity will only be contrasted within micro-hotplates from the same category, which we considered to be acceptable.

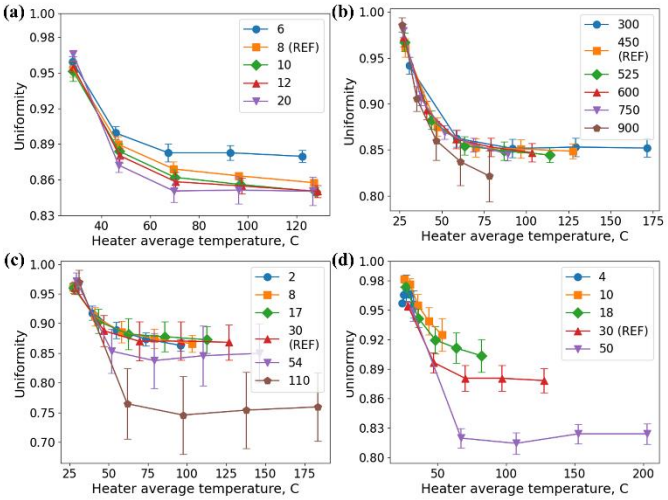

Fig. 7. Comparison of uniformity values for **(a)** microheaters with variable number of lines **(b)** microheaters with variable scaling **(c)** microheaters with variable line spacing and **(d)** microheaters with variable linewidth.

Thermal fluctuations coming from hotspots increase with the number of lines, therefore, the uniformity values are expected to decrease accordingly, as seen in Fig. 7a. The influence of the sizing is shown in Fig. 7b, which suggests that heaters with identical structures will maintain similar uniformity, regardless of their dimensions. Besides, increasing the space between heating lines leads to cold areas within the heater, as the heat will reach these regions with more difficulty. This is in agreement with the provided experimental results in Fig. 7c, showing a decrease in uniformity for spacing values greater than 30 µm. Lastly, Fig. 7d shows that uniformity worsens with increasing linewidth.

C. FEM model simulations

The origin of the temperature fluctuations can be better illustrated through FEM simulations, which were performed for each microheater design. The results of the reference meander are shown in Fig. 8 and includes a schematic of the model and mesh used (Fig. 8a), the electrical potential across the microheater when having one terminal biased to 3 V and the other terminal grounded (Fig. 8b), and its corresponding temperature profile in the surface of the microheater (Fig. 8c). Note in Fig. 8a-8c the square shapes distributed on top of the device active area, which account for the simulated temperature sensors. To obtain a detailed overview of the heat distribution at different voltages, we have extracted the temperature profile along the x-direction of the model surface marked as a red line in Fig. 8a, and the results are shown in Fig. 8d. The inset of this figure corresponds only to the microheater active area, thus ranging from a distance of *-d* to *d*. This last image illustrates the fluctuation of the temperature due to the hotspots, and the decrease in temperature in the edges, which were previously discussed in Section III.B The tails of the curves originate from the heat conduction through

the PI and they will be contrasted by the results obtained by the sensors in plane (see Section III.D).

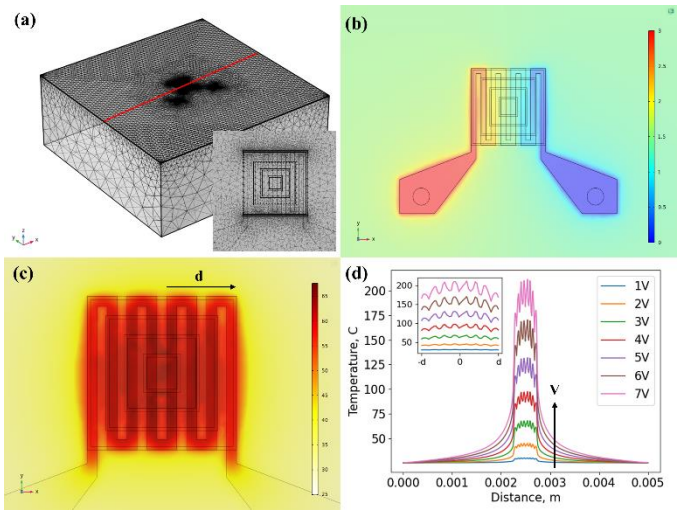

Fig. 8. Finite Element Simulations for the reference microheater. **(a)** Schematic of the model and mesh used. The inset corresponds to a zoom-in illustration of the device area. **(b)** Electric potential across the device, and **(c)** surface temperature for an applied voltage of 3 V. **(d)** Temperature profile for different voltages along the cross section marked as a red line in Fig. 8a.

The temperature profile of the microheaters with smallest spacing, largest spacing, smallest linewidth, and largest linewidth, is depicted in Fig. 9a, 9b, 9c, and 9d, respectively. Plots show the temperature profile from 1V to 7V, as it is the voltage range used for the experiments in the previous sections. These simulations show a clear influence of the linewidth and spacing on the temperature profile along the hotplate area. By designing microheaters with reduced spacing between the heating lines, a smooth temperature distribution can be obtained without the existence of hotspots (Fig. 9a). In opposition, strong thermal fluctuations are introduced if the line spacing is ample (Fig. 9b). Based on Fig. 9c and 9d, the width of the heating lines mainly determines the width of the hotspot peaks. Whereas in the 50 µm width microheater the hotspots are rather broad, for the 4 µm width microheater they appear as sharp temperature peaks. If Fig. 9c and 9d were superposed, one could see that for a given temperature, e.g. ~35 ºC, the amplitude of the peak is comparable. This suggests that the temperature in the hottest areas and colder areas is not influenced by the width of the lines. For all the depicted cases in Fig. 9, it should be noted that there is a strong edge effect, especially for the case of 2 µm spacing microheater.

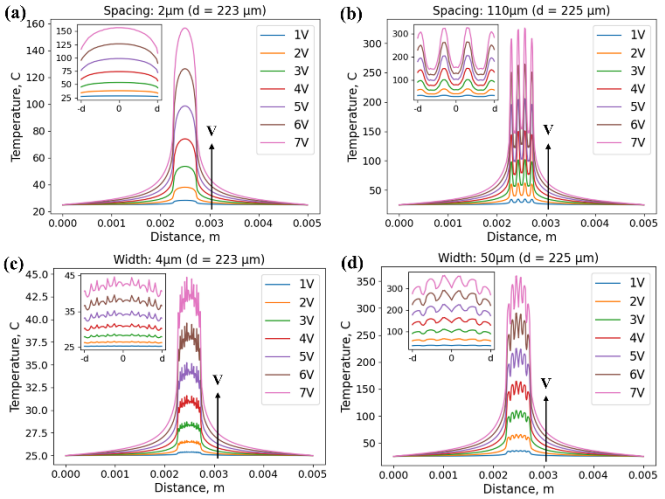

Fig. 9. Simulated temperature profile at different voltages of **(a)** 2 µm spacing microheater, **(b)** 110 µm spacing microheater, **(c)** 4 µm linewidth microheater, and **(d)** 50 µm spacing microheater.

To develop a meander-based microheater with high uniformity, an appropriate structure must be selected as such that the hotspots and edge effects are minimised. It is evident that the fluctuations coming from hotspots can be efficiently reduced by modulating linewidth, which is depicted in Fig. 9a. However, alternative strategies need to be applied to tackle the edge effects problem. A common approach among authors is to reduce the linewidth in the periphery of the microheater [5], [13], [17]. The reasoning is that since the current density will be maintained throughout the device, thinner and therefore more resistive lines will produce a greater heat dissipation, thus compensating for heat losses in the vicinity of the microheater.

D. FEM model validation using on-top and in-plane sensors

The importance of validating FEM simulations with the experimental results was previously discussed in depth. To this end, we compare the simulations of the reference microheater with the data extracted by both on-top sensors (Fig. 10) and in-plane sensors (Fig. 11) at different voltages.

In Fig. 10, the simulated thermal distribution in the x-direction of the heater's active area is represented as lines, whereas the circles correspond to the simulated sensors on top of the device (described in Fig. 8b). As is the case, the simulated temperature of the sensor (circles) does not have to exactly coincide with the actual horizontal temperature profile (lines). This arises from the fact that sensors take the temperature average of distinct regions and are exposed to hot and cold regions in the x-direction, i.e. the hotspot influence. The experimental results of the on-top sensors are represented in the figure as crosses with their corresponding error bars and are in excellent accord with the simulations. In this way, it is demonstrated that temperature sensor metrics could provide useful insight into the edge effect and, in a more indirect manner, into the hotspots.

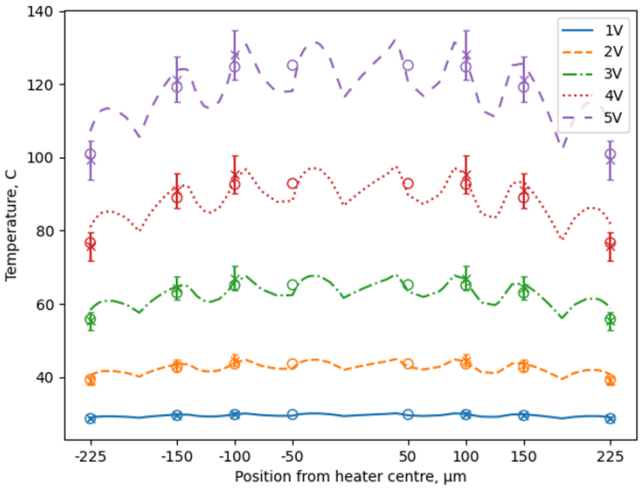

Fig. 10. On-top sensors, comparison of simulations and experimental data at different points of the microheater's active area. Lines (dash, dotted, etc.) represent the simulated temperature profile along the horizontal cross section, circles represent simulated sensor temperatures, and crosses represent the sensor temperatures extracted experimentally.

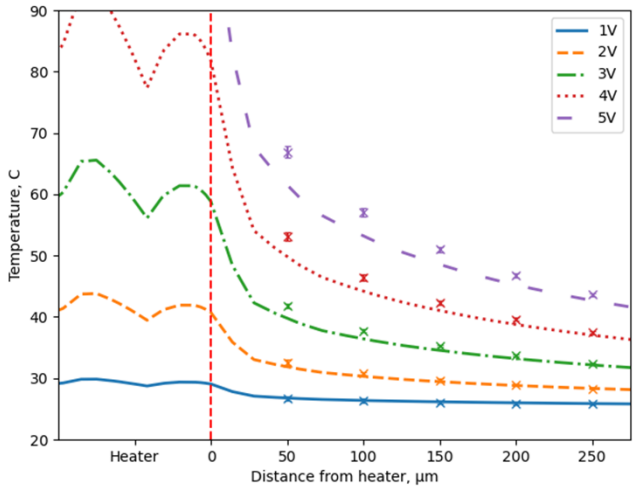

Fig. 11. In-plane sensors, comparison of simulations and experimental data at different distances from the heater. Lines (dash, dotted, etc.) represent the simulated temperature profile along the horizontal cross section, and crosses represent the sensor temperature extracted experimentally.

On the other hand, Fig. 11 presents zoom-in view of the heat conduction tail away from the hotplate, where lines represent the temperature obtained by simulations. The vertical dashed red line establishes the boundaries of the device's active area. From the figure, we can observe that the temperature decays exponentially along the PI. This exponential behavior has already been reported in the literature in the work of Simon I. *et al.* [20]. where they make use of a one-dimensional heat conduction equation in cylindrical coordinates, under the assumption that the microheater can be described with circular geometry. The experimental data derived from in-plane sensors are superimposed on the graph, represented as crosses with their corresponding error bars. Similarly, simulations align well with the observed experimental data. Comparable results have been found for all the other studied micro-hotplates.

To evaluate the accuracy of the sensors for the validation of our FEM model, simulations were conducted with variations in the heat transfer mechanism parameters (see Fig. 12).

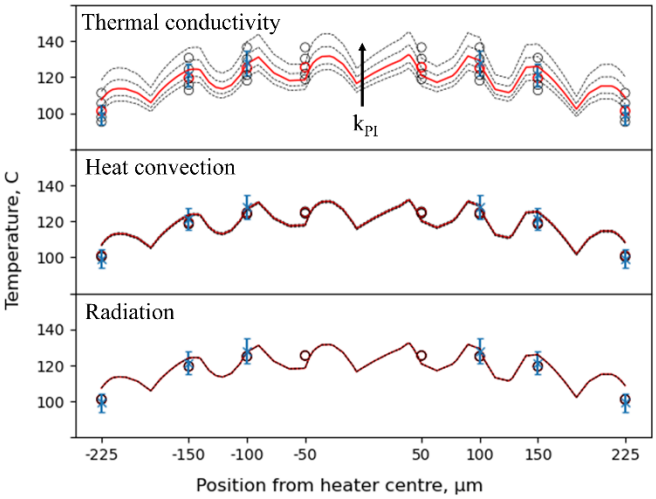

Fig. 12. Comparison of experimental results (blue) and simulations (black) using different heat transfer assumptions at 5V. The simulation that contains the original parameters is highlighted in solid red. Modulated parameters are **(top)** PI thermal conductivity, k_{PI} = 0.11, 0.13, 0.15, 0.17 and 0.19 W/(m K), **(middle)** heat transfer coefficient, h = 0, 10, 20, 30 and 40 W/(m^2 K), and **(bottom)** PI emmisivity of ε = 0.65, 0.70, 0.75, 0.80 and 0.85.

For these, the supplied voltage was maintained at a value of 5V. The original simulation parameters are highlighted in the figure and the text in red and bold, respectively. The impact on heat conduction was addressed by varying the thermal conductivity of the polyimide insulator (*kPI*) to values of 0.11, 0.13, **0.15**, 0.17 and 0.19 W/(m K) (top figure). The contribution of heat convection was studied by performing simulations with h = 0, **10**, 20, 30 and 40 W/(m^2 K), which are values that fall in a free convection regime (middle figure). The influence of radiation is studied by modifying the emissivity of the polyimide, to values of ε = 0.65, 0.70, **0.75**, 0.80 and 0.85 (bottom figure). For our system and under the considered values, it is demonstrated that the major contribution to power dissipation relies on the heat conductivity of the insulator, likely arising from the considerable thickness of PI. As depicted in the graphic, the use of an insulator with lower thermal conductivity limits the temperature at the microheater surface, however, it will improve the uniformity as a result of the reduction of the hotspot amplitude. Compared with the experimental results, the most fitting kPI value is the one originally used. Heat convection and radiation, on the other hand, are minor contributors to our system, i.e. the selection of the different parameters has little impact on the temperature profile. Thus, we could assume that our original FEM model can be effectively used to describe our experimental conditions, and therefore is valid. Importantly, we should remark that the

contributions of the heat transfer mechanisms may vary from system to system depending on material selection, microheater geometry or measurement conditions. If the system is driven by another mechanism, or by a combination or mechanisms, an increase in sensitivity should be expected towards the corresponding parameters. And consequently, the validation of the model using the thermal sensors could be more precise for those contributions.

With these results, we have demonstrated that the assumptions made for the simulations are representative. Furthermore, we have provided evidence that the use of thermal sensors serves as a tool to experimentally extract the thermal profile in the regions of interest and obtain experimental insight in the uniformity.

E. Sensor applicability: considerations and limitations

From a practical point of view, some aspects and limitations need to be explained more thoroughly. Firstly, we should examine the robustness of the sensor readings. For that, it is crucial to first ensure consistent microheater characteristics, which can be confirmed considering the low measurement deviation from Fig. 3 - Fig. 6. The precision of the sensor readings decreases with the temperature as seen by the error bars from Fig. 10, with a typical measurement deviation of less than 5%. Exceptions to this are found in the samples with spacing of 54 µm (6%) and 110 µm (7%), which also show higher variability in the calculated uniformity (Fig. 7). Despite this, thermal sensors can still achieve good accuracy when considering the average value, as seen in Fig. 10. Devices with identical characteristics (i.e the reference heaters) yield an equivalent average result with a percentage difference of 2%, suggesting that the sensors readings are reproducible.

Secondly, it is important to consider sensor's resolution and sensitivity. The sensor responds to the average temperature of the area they cover, so the resolution is limited to their width, which in our case was of 10 µm. Reducing the sensor width could effectively improve the resolution, however, care must be taken to maintain sufficiently low current values to avoid self-heating. Due to the selection of platinum as sensing material, the sensitivity of the sensor readings is limited to a an ideal value of 0.39%/C. If required, this could be enhanced by selecting materials with higher TCR. Furthermore, the sensors are more sensitive to edge effect contributions owing to their design. Notwithstanding, the applicability of the sensors can be further extended if the design is adapted. For example, a set of small sensors centered in different regions of the microheater could map the surface in a more effectively way. Else, sensors fully placed in cold or hot areas that could give a more direct experimental indication of hotspots.

Thirdly, the completeness of the measurements needs to be discussed. To demonstrate the concept of the paper, we limited our investigations to a very small sets of sensors. For practical applications, however, it would be necessary to increase the number of sensors (8-10 sensors) in order to obtain a more complete thermal profile. This would also lead to a more realistic uniformity value and possibly a more accurate validation of the FEM model. The main drawback in this approach would be the more space consumed on the wafer and the additional design efforts required.

The output of this paper can be especially valuable for researchers who need to design and characterize microheaters with high uniformity. Microheaters with uniform thermal distribution are a key component in applications which need exceptional temperature control, such as microfluidics [34], [35] , DNA amplification [36], and cell culture [37]. Besides, microheaters are widely used in gas sensing field, especially for metal oxide semiconductor sensors that require high operating temperatures [38]. In this context, the use of micro hotplates in gas sensors could be further extended to other type of sensors [3], [39] as a tool to I) maintain a constant and uniform temperature, which is crucial to detecting gases accurately, and II) provide an effective way to remove the gases by means of heat pulses.

CONCLUSIONS

This paper has provided three key contributions:

- An innovative alternative to extract experimental information on microheater uniformity. For that, we on-top sensors were designed in such a way as to measure the average temperature in equidistant regions from the active area edges, thus giving a direct insight into the edge effect. Moreover, the measured average temperature also provided indirect information of the hotspots, which could be better resolved with a validated FEM model.

- A methodology to verify if a FEM model is appropriate to describe the experiment in a realistic way. On-top sensors provided information into the suitability of the assumptions in heat conduction, convection and radiation. In-plane sensors were used as a complementary tool to study the assumptions in the heat conduction through the insulator. We obtained good resemblance between experiments and simulations.

- An overview on the influence of microheater geometry on its thermal characteristics and uniformity. This can serve as a guide to design meander-based structures according to the required application.

Furthermore, the characteristics of the sensors, including robustness, sensitivity, and completeness, are discussed. To achieve more accurate results, we recommend increasing the number of sensors. Additionally, the sensor design can be customized to prioritize other uniformity contributions, or to accommodate other microheater geometries.

ACKNOWLEDGEMENTS

M. Calderon-Gonzalez is thankful to Tibor Kuna and Myriam Willegems for their help provided regarding the fabrication process. Epimitheas Georgitzikis and Max L. Tietze are acknowledged for their scientific guidance. Frederik Hanssen, Bart Aerts, Anastasia Glushkova, and Anton

Gavrilov are acknowledged for their support regarding characterization tools.

REFERENCES

[1] E. Mavraki, D. Moschou, G. Kokkoris, N. Vourdas, S. Chatzandroulis, and A. Tserepi, "A continuous flow μPCR device with integrated microheaters on a flexible polyimide substrate," *Procedia Engineering*, vol. 25, pp. 1245–1248, 2011, doi: 10.1016/j.proeng.2011.12.307.

[2] J. Cho and G. Shin, "Fabrication of a Flexible, Wireless Micro-Heater on Elastomer for Wearable Gas Sensor Applications," *Polymers*, vol. 14, no. 8, Art. no. 8, Jan. 2022, doi: 10.3390/polym14081557.

[3] M. R. Venkatesh *et al.*, "A Low-Power MEMS IDE Capacitor with Integrated Microhotplate: Application as Methanol Sensor using a Metal-Organic Framework Coating as Affinity Layer," *Sensors*, vol. 19, no. 4, Art. no. 4, Jan. 2019, doi: 10.3390/s19040888.

[4] S. Yu, S. Wang, M. Lu, and L. Zuo, "A novel polyimide based micro heater with high temperature uniformity," *Sensors and Actuators A: Physical*, vol. 257, pp. 58–64, Apr. 2017, doi: 10.1016/j.sna.2017.02.006.

[5] J. Courbat, M. Canonica, D. Teyssieux, D. Briand, and N. F. de Rooij, "Design and fabrication of micro-hotplates made on a polyimide foil: electrothermal simulation and characterization to achieve power consumption in the low mW range," *J. Micromech. Microeng.*, vol. 21, no. 1, p. 015014, Dec. 2010, doi: 10.1088/0960-1317/21/1/015014.

[6] S. K. Tiwari, S. Bhat, and K. K. Mahato, "Design and fabrication of screen printed microheater," *Microsyst Technol*, vol. 24, no. 8, pp. 3273–3281, Aug. 2018, doi: 10.1007/s00542-018-3821-6.

[7] Z. E. Jeroish, K. S. Bhuvaneshwari, F. Samsuri, and V. Narayanamurthy, "Microheater: material, design, fabrication, temperature control, and applications—a role in COVID-19," *Biomed Microdevices*, vol. 24, no. 1, p. 3, Dec. 2021, doi: 10.1007/s10544-021-00595-8.

[8] P. Bhattacharyya, "Technological Journey Towards Reliable Microheater Development for MEMS Gas Sensors: A Review," *IEEE Transactions on Device and Materials Reliability*, vol. 14, no. 2, pp. 589–599, Jun. 2014, doi: 10.1109/TDMR.2014.2311801.

[9] U. Khan and C. Falconi, "Temperature distribution in membrane-type micro-hot-plates with circular geometry," *Sensors and Actuators B: Chemical*, vol. 177, pp. 535–542, Feb. 2013, doi: 10.1016/j.snb.2012.11.007.

[10] S. M. Lee, D. C. Dyer, and J. W. Gardner, "Design and optimisation of a high-temperature silicon micro-hotplate for nanoporous palladium pellistors," *Microelectronics Journal*, vol. 34, no. 2, pp. 115–126, Feb. 2003, doi: 10.1016/S0026-2692(02)00153-2.

[11] X. Lu *et al.*, "Design and Fabrication of a Novel Poly-Si Microhotplate with Heat Compensation Structure," *Micromachines*, vol. 13, no. 12, Art. no. 12, Dec. 2022, doi: 10.3390/mi13122090.

[12] G. Pühringer, B. Jakoby, T. Söllradl, C. Ranacher, S. Lodha, and T. Grille, "Characterization of silver microheaters for vertical-cavity enhanced resonant thermal emission," in *2017 IEEE SENSORS*, Oct. 2017, pp. 1–3. doi: 10.1109/ICSENS.2017.8234377.

[13] G. Velmathi, N. Ramshanker, and S. Mohan, "Design, Electro-Thermal simulation and geometrical optimization of double spiral shaped microheater on a suspended membrane for gas sensing," in *IECON 2010 - 36th Annual Conference on IEEE Industrial Electronics Society*, Nov. 2010, pp. 1258–1262. doi: 10.1109/IECON.2010.5675550.

[14] D. Li, Y. Ruan, C. Chen, W. He, C. Chi, and Q. Lin, "Design and Thermal Analysis of Flexible Microheaters," *Micromachines*, vol. 13, no. 7, Art. no. 7, Jul. 2022, doi: 10.3390/mi13071037.

[15] J. Wang, D. Yang, T.-L. Chang, P. Cui, Y. Duan, and W. Ye, "Optimization Design of Flexible Gas Senor Microheater," in *2020 21st International Conference on Electronic Packaging Technology (ICEPT)*, Aug. 2020, pp. 1–4. doi: 10.1109/ICEPT50128.2020.9202656.

[16] M. Gayake, D. Bodas, and S. Gangal, "Simulations of Polymer based Microheater Operated at Low Voltage".

[17] Q. Liu, G. Ding, Y. Wang, and J. Yao, "Thermal Performance of Micro Hotplates with Novel Shapes Based on Single-Layer SiO2 Suspended Film," *Micromachines*, vol. 9, no. 10, Art. no. 10, Oct. 2018, doi: 10.3390/mi9100514.

[18] S. Joy and J. K. Antony, "Design and Simulation of a Micro Hotplate Using COMSOL Multiphysics for MEMS Based Gas Sensor," in *2015 Fifth International Conference on Advances in Computing and Communications (ICACC)*, Sep. 2015, pp. 465–468. doi: 10.1109/ICACC.2015.108.

[19] C. Paun, R. Tomescu, D. Cristea, O. Ionescu, and C. Parvulescu, "Design, fabrication and caracterization of a micro-heater for metasurface-based gas sensors," in *2020 International Semiconductor Conference (CAS)*, Oct. 2020, pp. 31–34. doi: 10.1109/CAS50358.2020.9267975.

[20] I. Simon, N. Bârsan, M. Bauer, and U. Weimar, "Micromachined metal oxide gas sensors: opportunities to improve sensor performance," *Sensors and Actuators B: Chemical*, vol. 73, no. 1, pp. 1–26, Feb. 2001, doi: 10.1016/S0925-4005(00)00639-0.

[21] R. G. Spruit, J. T. van Omme, M. K. Ghatkesar, and H. H. P. Garza, "A Review on Development and Optimization of Microheaters for High-Temperature In Situ Studies," *Journal of Microelectromechanical Systems*, vol. 26, no. 6, pp. 1165–1182, Dec. 2017, doi: 10.1109/JMEMS.2017.2757402.

[22] J. Kang *et al.*, "Temperature control of micro heater using Pt thin film temperature sensor embedded in micro gas sensor," *Micro and Nano Systems Letters*, vol. 5, no. 1, p. 26, Sep. 2017, doi: 10.1186/s40486-017-0060-z.

[23] G. Keshavaditya, G. R. Eranna, and G. Eranna, "PRT Embedded Microheaters for Optimum Temperature Distribution of Air-Suspended Structures for Gas Sensor Applications," *IEEE Sensors Journal*, vol. 15, no. 7, pp. 4137–4140, Jul. 2015, doi: 10.1109/JSEN.2015.2413835.

[24] A. S. Algamili *et al.*, "Fabrication and Characterization of the Micro-Heater and Temperature Sensor for PolyMUMPs-Based MEMS Gas Sensor," *Micromachines*, vol. 13, no. 4, Art. no. 4, Apr. 2022, doi: 10.3390/mi13040525.

[25] H.-S. Chuang and S. Wereley, "Design, fabrication and characterization of a conducting PDMS for microheaters and temperature sensors," *J. Micromech. Microeng.*, vol. 19, no. 4, p. 045010, Mar. 2009, doi: 10.1088/0960-1317/19/4/045010.

[26] J.-W. Han and M. Meyyappan, "A Built-In Temperature Sensor in an Integrated Microheater," *IEEE Sensors Journal*, vol. 16, no. 14, pp. 5543–5547, Jul. 2016, doi: 10.1109/JSEN.2016.2569445.

[27] M. Yin *et al.*, "3D Printed Microheater Sensor-Integrated, Drug-Encapsulated Microneedle Patch System for Pain Management," *Advanced Healthcare Materials*, vol. 8, no. 23, p. 1901170, 2019, doi: 10.1002/adhm.201901170.

[28] A. Sharma and B. Sharma, "Influence of microheater patterns: MoSi2-SnO2 as energy-saving chemiresistors for gas sensing applications," *Sensors and Actuators B: Chemical*, vol. 351, p. 130901, Jan. 2022, doi: 10.1016/j.snb.2021.130901.

[29] F. Jiang, L. Schaller, M. Ryu, J. Morikawa, S. Ingebrandt, and X. T. Vu, "Micro-Joule heater and temperature sensor array on a suspended silicon nitride membrane for measurement of in-plane thin film thermal diffusivity," *Sensors and Actuators A: Physical*, vol. 362, p. 114635, Nov. 2023, doi: 10.1016/j.sna.2023.114635.

[30] M. R. Adib, V. V. Kondalkar, and K. Lee, "Development of Highly Sensitive Ethane Gas Sensor Based on 3D WO3 Nanocone Structure Integrated with Low-Powered In-Plane Microheater and Temperature Sensor," *Advanced Materials Technologies*, vol. 5, no. 5, p. 2000009, 2020, doi: 10.1002/admt.202000009.

[31] J. Han, Z. Tan, K. Sato, and M. Shikida, "Thermal characterization of micro heater arrays on a polyimide film substrate for fingerprint sensing applications," *J. Micromech. Microeng.*, vol. 15, no. 2, p. 282, Nov. 2004, doi: 10.1088/0960-1317/15/2/006.

[32] M. Horade, M. Kojima, K. Kamiyama, Y. Mae, and T. Arai, "Development of a Novel 2-Dimensional Micro-Heater Array Device with Regional Selective Heating," *MER*, vol. 6, no. 1, p. 66, Apr. 2016, doi: 10.5539/mer.v6n1p66.

[33] J. Courbat, D. Briand, and N. F. de Rooij, "Reliability improvement of suspended platinum-based micro-heating elements," *Sensors and Actuators A: Physical*, vol. 142, no. 1, pp. 284–291, Mar. 2008, doi: 10.1016/j.sna.2007.04.006.

[34] V. Selvakumar, S. Suganthi, S. Lakshmi Narayanan, and C. Gayathri, "Microfabrication and Evaluation of a Novel Micro Electro Mechanical System Based Polysilicon Microheater for Microfluidic Applications," *Sensor Letters*, vol. 17, pp. 474–480, Jun. 2019, doi: 10.1166/sl.2019.4086.

[35] J. M. Son, J. H. Lee, J. Kim, and Y. H. Cho, "Temperature distribution measurement of Au micro-heater in microfluidic channel using IR microscope," *Int. J. Precis. Eng. Manuf.*, vol. 16, no. 2, pp. 367–372, Feb. 2015, doi: 10.1007/s12541-015-0048-7.

[36] T.-M. Hsieh, C.-H. Luo, F.-C. Huang, J.-H. Wang, L.-J. Chien, and G.-B. Lee, "Enhancement of thermal uniformity for a microthermal cycler and its application for polymerase chain reaction," *Sensors and Actuators B: Chemical*, vol. 130, no. 2, pp. 848–856, Mar. 2008, doi: 10.1016/j.snb.2007.10.063.

[37] J.-L. Lin, M.-H. Wu, C.-Y. Kuo, K.-D. Lee, and Y.-L. Shen, "Application of indium tin oxide (ITO)-based microheater chip with uniform thermal distribution for perfusion cell culture outside a cell incubator," *Biomed Microdevices*, vol. 12, no. 3, pp. 389–398, Jun. 2010, doi: 10.1007/s10544-010-9395-4.

[38] "Micromachines | Free Full-Text | Microhotplates for Metal Oxide Semiconductor Gas Sensor Applications—Towards the CMOS-MEMS Monolithic Approach." Accessed: Jul. 24, 2024. [Online]. Available: https://www.mdpi.com/2072-666X/9/11/557

[39] R. Hopper, D. Popa, F. Udrea, S. Z. Ali, and P. Stanley-Marbell, "Miniaturized thermal acoustic gas sensor based on a CMOS microhotplate and MEMS microphone," *Sci Rep*, vol. 12, no. 1, p. 1690, Feb. 2022, doi: 10.1038/s41598-022-05613-0.

Maider Calderon Gonzalez was born in Guipuzkoa, Spain, in 1996. She received her B.Sc. degree in chemistry at the Universidad Autonoma de Madrid (2019), and her M.Sc. degree in nanoscience, nanotechnology, and nanoengineering at Katholieke Universiteit Leuven (2021). During her bachelor's degree she was hosted in the group of Imo-Imomec at Hasselt Universiteit, where she completed an internship and bachelor thesis regarding the development of perovskites for photovoltaic applications. Afterwards, she joined the cMACs group at KU Leuven to perform her master's thesis on chemical vapor deposition of ionic liquids. Since 2021, M. Calderon Gonzalez is pursuing a Ph.D. on the development of highly sensitive and selective gas sensors for monitoring volatile organic compounds. This Ph.D. is positioned between KU Leuven and Imec. Her current research includes the design, fabrication, and characterization of microheaters and thin-film transistors; and the investigation of gas adsorption of porous materials.

David Cheyns received his master and Ph.D. in electrical engineering in 2003 and 2008, respectively, from the Katholieke Universiteit Leuven, Belgium. He has over 20 years' experience in thin-film, large-area technologies, and co-authored over 50 publications and 5 patents. He was co-organizer of SPIE Europe, eMRS and member of the scientific advisory board of EUPV-SEC. He pioneered the work on organic tandem solar cells, perovskite materials, OLEDs, colloidal quantum dots and thin-film photovoltaic modules at imec. Presently, he is R&D manager in the "Sensor and Actuator Technologies" department. In this role, he is responsible for the development of next-generation sensors and actuators for applications such as infrared imaging, gesture recognition, medical imaging, haptic feedback and microfluidics.

Rob Ameloot obtained his PhD in 2011 at KU Leuven (Belgium) and was a Fulbright postdoctoral fellow at UC Berkeley (US). Currently, he is a tenured professor at KU Leuven. He was awarded ERC Consolidator, Starting, and Proof-of-Concept grants to bring microporous materials from the chemistry lab into the microelectronics fab. In general, he is passionate about pushing the envelope in porous materials and their applications, with a healthy disregard for traditional subject boundaries.

Jan Genoe (Member, IEEE) is born in Leuven, Belgium, in 1965. He received the M.S. degree in electrical engineering and the Ph.D. degree from the KU Leuven, Leuven, in 1988 and 1994, respectively. After his Ph.D., he joined the High Magnetic Field Laboratory, Grenoble, France, as a Human Capital and Mobility Fellow of the European Community. In December 1997, he became an Assistant Professor and in September 2000, he became an Associate Professor with the KHLim, Diepenbeek, Belgium. In September 2003, he also became In Charge of the Polymer and Molecular Electronics Group, imec, Leuven. His subsequent carrier steps in imec have been the Principal Scientist, a Senior Principal Scientist, and a Chief Scientist with the LAE Department, imec. He is currently the Scientific Director of the Sensors and Actuators Technology Department, imec and a part-time Full-Professor with the KU Leuven. His current research interests include the combination of novel devices with design in novel technologies. A crucial aspect when designing using emerging technologies is the careful assessment of parameter variations in the device characteristics. This technology insight, combined with creative design variations, has enabled an increase in the level of complexity that can be obtained using designs in organic and oxide technology. Examples of design modifications to accommodate technology are the usage of a back-gate to adapt the threshold voltages and the alternative modulation scheme to obtain bidirectional communication in thin-film RFID tags. This work has resulted in ten subsequent International Solid-State Circuits Conference (ISSCC) presentations in the Technology Directions Session (e.g., 128-bit organic RFID tags, organic microprocessors, and hybrid oxide-organic RFID tags). Other emerging technologies such as organic photovoltaics, piezo-electric devices, high-resolution imagers comprising features below the wavelength of the light and holography are also currently being investigated. Dr. Genoe received an Advanced Grant from the European Research Council (ERC) on the topic of new metamaterials for holography, in 2017. He is a reviewer for a broad range of journals (e.g., Electrochemical and Solid State Letters, Electron Device Letter, Thin Solid Films, Journal of Applied Physics, Semiconductor Science and Technology, Electronics Letters, and Organic Electronics) and has been a member for five years of the Technology Directions International Program Committee of the ISSCC.